

Modelling the chemical evolution of molecular clouds as a function of metallicity

E. M. Penteado^{1*}, H. M. Cuppen¹ and H. J. Rocha-Pinto²

¹*Institute for Molecules and Materials, Radboud University Nijmegen Heyendaalsweg 135, 6525 AJ Nijmegen, The Netherlands*

²*UFRJ, Observatório do Valongo, Ladeira Pedro Antônio 43, 20080-090, Rio de Janeiro, Brazil*

20 August 2019

ABSTRACT

The Galaxy is in continuous elemental evolution. Since new elements produced by dying stars are delivered to the interstellar medium, the formation of new generations of stars and planetary systems is influenced by this metal enrichment. We aim to study the role of the metallicity on the gas phase chemistry of the interstellar medium. Using a system of coupled-ordinary differential equations to model the chemical reactions, we simulate the evolution of the abundance of molecules in the gas phase for different initial interstellar elemental compositions. These varying initial elemental compositions consider the change in the “elemental abundances” predicted by a self-consistent model of the elemental evolution of the Galaxy. As far as we are aware, this is the first attempt to combine elemental evolution of the Galaxy and chemical evolution of molecular clouds. The metallicity was found to have a strong effect on the overall gas phase composition. With decreasing metallicity, the number of long carbon chains was found to increase, the times-scale on which small molecular species are increases, and the main form of oxygen changed from O and CO to O₂. These effects were found to be mainly due to the change in electron, H₃⁺, and atomic oxygen abundance.

Key words: astrochemistry – ISM: abundances – ISM: molecules.

1 INTRODUCTION

Molecular clouds are chemically rich environments where over 180 molecular species have been observed and these are the sites of star and planet formation (Herbst & van Dishoeck 2009).

* E-mail: e.monfardini@science.ru.nl

Molecules play a central role in determining the thermal budget of astrophysical bodies and provide crucial building blocks during star and planet formation. The understanding of such environments has always been a challenge and, for decades, astrochemists have developed different models to describe the rich and complex chemistry of the interstellar medium (ISM), which might consider only reactions occurring in the gas phase (Herbst & Klemperer 1973) or also chemistry taking place on the surfaces of interstellar dust grains (Tielens & Hagen 1982). Although it is well known that many molecules are more efficiently formed on the surface of astrophysical ices, gas phase chemistry has an important role on the chemical evolution of dense molecular clouds and its study is still necessary to deepen our knowledge about the evolution of the ISM. Models to describe gas phase (*e.g.* Wakelam et al. 2012) and grain surface chemistry (*e.g.* Vasyunin & Herbst 2013) of the ISM are continuously elaborated and are improved by comparisons with laboratory results and with observations.

The most commonly used method to model interstellar gas phase chemistry is based on reaction rate equations. In this method, a set of ordinary coupled differential equations, in which each equation describes the time variation of the concentration of a molecule, is built accordingly to the reactions under consideration. This set of differential equations can only be solved numerically and the number of equations follows the number of species considered, typically hundreds, which are normally connected by thousands of reactions. The final aim of astrochemical models is to understand how the abundances of the molecules change with time according to a set of initial abundances and to a set of astrophysical parameters.

Many molecules are expected to be discovered in the near future because of the development of a new generation of ground-base interferometers, like the Atacama Large Millimeter/submillimeter Array (ALMA), forcing the development of new models able to describe such complex environment in more details. Moreover, these instruments will allow us to look at the molecular complexity beyond our own Galaxy, probably even at higher redshift. Studies of formation of simple molecules at high redshift have been developed (Cazaux & Spaans 2009) and detection of molecules in extragalactic sources has already been reported (Pereira-Santaella et al. 2013, and references therein).

The present work presents simulations of the variation of abundances of molecules in a cold dense molecular cloud computed by taking into account the elemental evolution of the Galaxy. Wakelam et al. (2010) have also studied the effect of the change in the initial elemental abundances and other input parameters but, differently from our study, their choice of the initial abundances did not take into account the elemental evolution of the Galaxy. Elements heavier than hydrogen

and helium are delivered to the ISM during stellar deaths. This process continuously enriches molecular clouds so that new generations of stars and planetary systems are born with a different initial elemental composition. To this process of element formation and delivery to the ISM, we refer as “elemental evolution of the Galaxy”. To the production and evolution of molecules in dense cold molecular clouds, we refer as “chemical evolution”¹. Figure 1 shows schematically how the production of new elements by dying stars influences the production of molecules deeply inside dense and cold molecular clouds. The elemental evolution of the Galaxy can be interpreted as a clock, in which the metallicity, denoted by $[\text{Fe}/\text{H}]$, increases as time passes, so that the Galaxy must be more rich in metals in late than in early times. This can also be thought of in terms of redshift, so that galaxies at higher redshift must have lower metallicity, whereas galaxies at lower redshifts must have higher metallicity. Therefore, the metallicity represents a chronometer, which describes the accumulation of iron in the ISM. Wheeler, Sneden & Truran (1989) have already noted that the accumulation of iron in the ISM increases monotonically with time. Therefore, by connecting the elemental evolution of the Galaxy with the chemical evolution of the ISM, the study of the chemistry occurring in primordial gas of higher redshift is possible, as well as a comparison to the chemistry of present higher metallicity gas.

As mentioned before, we will limit our study to gas phase chemical models. Ultimately, one would like to repeat this study applying a full gas-grain model. However, a pure gas phase chemical model will be a good first step in understanding the influence of redshift on the gas phase composition. It is a representative model of quiescent cold clouds. Grains will mostly contribute in depleting the gas phase from certain species, but this is more dominant at high densities ($> 10^5 \text{cm}^{-3}$), and in the formation of new molecules that will enter the gas phase in later stages of the star formation sequence where the grains heat up and release their ice mantles. In the present study we will therefore limit ourselves to description of the gas phase composition at cold cloud conditions and we aim to understand how the gas phase chemistry changes with metallicity. We will further speculate on the possible further reactions that could occur on the grain surfaces. One might ask whether it is reasonable to study the galactic chemistry without considering the presence of grains. Gas–grain models are still in development and many issues still wait to be solved. The present work is the first attempt to combine both elemental and molecular evolution, connecting two dif-

¹ Since this work tracks both elemental and molecular evolution, we decided to use the term “chemical evolution” to refer only to the evolution of the abundance of molecules in clouds and “elemental evolution” to refer to the production of elements by dying stars. Therefore, the term “elemental evolution” is a synonymous for the term “chemical evolution” used by other authors.

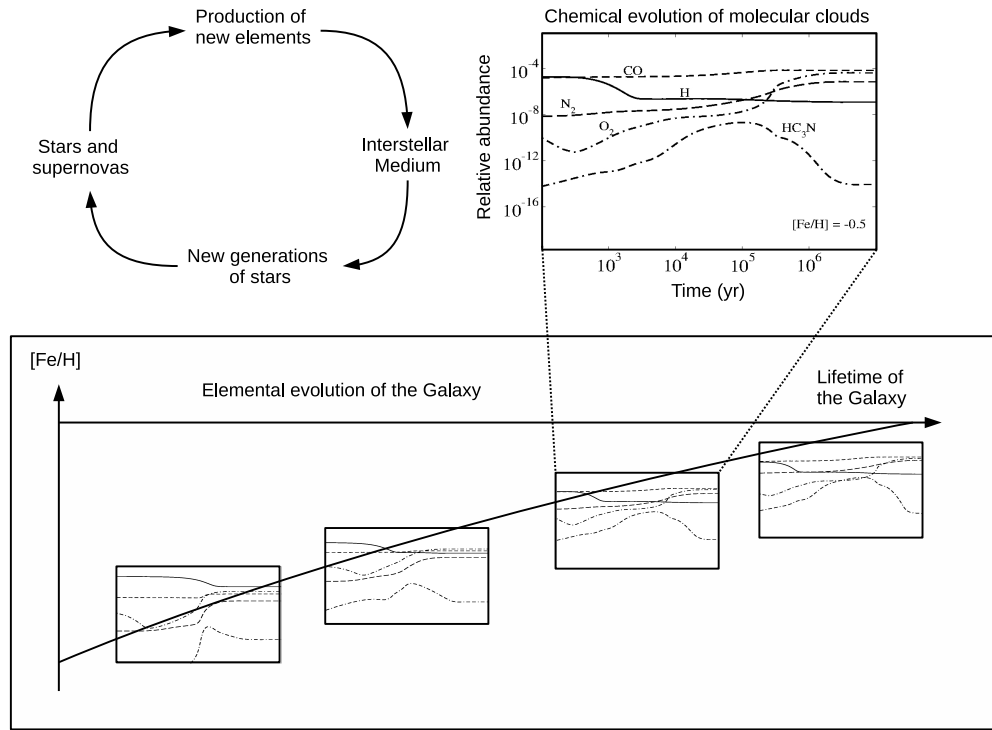


Figure 1. Chemical evolution of molecular clouds connected to the elemental evolution of the Galaxy. Top-left: schematic representation of the process of production and delivery of new elements to the ISM. Top-right: an example of chemical evolution of a molecular cloud for one specific metallicity. Bottom: representation of the elemental evolution of the Galaxy, where molecular clouds evolve with different initial metallicity along the life time (redshift) of the Galaxy.

ferent formalisms. This brings the necessity of starting with simple considerations, like excluding, for now, the presence of grains.

Details of the method and the process to find the initial elemental composition are described in Sec. 2, while the results and discussion are presented in Sec. 3. Finally, Sec. 4 gives our concluding remarks.

2 METHOD

The applied method consists of three steps: first, the initial abundances of a selection of elements are determined on the basis of a standard self-consistent model for the elemental evolution of the Galaxy described by Timmes, Woosley & Weaver (1995). These abundances are then depleted to account for the dust and finally given to a chemical code which calculates the time dependent chemical evolution of the molecular cloud.

2.1 Initial elemental abundances

The initial elemental abundances as a function of metallicity were obtained from a model for the elemental evolution of the Galaxy presented by Timmes, Woosley & Weaver (1995). These authors simulated the production of 76 stable isotopes by Type I and II supernovae, from hydrogen to zinc, through a dynamical and chemical model for the Galaxy, where they present the evolution of such elements with respect to the metallicity, *i.e.* $[X/Fe]$ versus $[Fe/H]$. The relation $[Fe/H]$ is used as a measure for the metallicity, which is defined as

$$\left[\frac{Fe}{H} \right] = \log \left[\frac{\epsilon(Fe)}{\epsilon(H)} \right] - \log \left[\frac{\epsilon(Fe)}{\epsilon(H)} \right]_{\odot}. \quad (1)$$

This equation compares the logarithms of the abundances of Fe and H, $\epsilon(Fe)$ and $\epsilon(H)$ respectively, in the molecular cloud under consideration (first term) and solar abundances (second term). The $[Fe/H]$ ratio can be interpreted as a chronometer which describes the accumulation of iron in the ISM. Timmes, Woosley & Weaver (1995) covered the scale from -3.0 to 0.0 , where $[Fe/H] = 0$ clearly represents solar metallicity. Our model covers an approximate range, from -2.5 to 0.0 . In terms of oxygen abundance, this range corresponds to $6.19 \leq \log(O/H) + 12 \leq 8.69$, where the first refers to $[Fe/H] = -2.5$ and the latter to solar metallicity (Asplund et al. 2009). Apart from their standard model to describe the elemental evolution, they made two refinements: $[N/Fe]$ calculated with convective overshoot and $[X/Fe]$ calculated with a factor of 2 in the iron yields. This leads to a total of four different sets of elemental abundances

- (1) the standard model;
- (2) same as (1) but $[N/Fe]$ calculated with convective overshoot;
- (3) $[X/Fe]$ calculated with a factor of 2 in the iron yields, but without convective overshoot;
- (4) same as (3), but with convective overshoot.

At solar metallicity these sets coincide. The largest difference between the sets is for nitrogen at high redshift; the standard model predicts a very low nitrogen abundance under these conditions. Observations suggest that nitrogen is primarily produced in low-metallicity massive stars, and Timmes, Woosley & Weaver (1995) could only reproduce this by artificially enlarging the numerical parameter which treats convective overshoot (models 2 and 4). When applying this, the nitrogen abundance increases with several orders of magnitude, in better agreement with the observations. In general, model (4) gives the best agreement with observational data for all elements and we therefore use this model to obtain the abundance of all elements throughout this study.

There are however a few exceptions. This is the case for phosphorus and chlorine. The dominant molecular forms of these elements show only weak lines in synthetic stellar spectra, making it

difficult to determine their abundances in dwarf or field giants. For this reason, Timmes, Woosley & Weaver (1995) used only their standard calculations to predict the chlorine and phosphorus abundances relative to iron. These calculations were used in this work to predict the initial abundances of these elements for all models.

The program NAHOON (Wakelam et al. 2012), which is used to simulate the chemical evolution of a particular molecular cloud, requires elemental abundances to be provided with respect to hydrogen and these values are obtained using

$$\left[\frac{X}{H}\right] = \left[\frac{X}{Fe}\right] + \left[\frac{Fe}{H}\right], \quad (2)$$

and considering the definition

$$\left[\frac{X}{H}\right] = \log \left[\frac{\varepsilon(X)}{\varepsilon(H)}\right] - \log \left[\frac{\varepsilon(X)}{\varepsilon(H)}\right]_{\odot}, \quad (3)$$

where $\varepsilon(X)$ is the abundance of certain element. Solar abundances are taken from Asplund et al. (2009) and are reproduced in Table 1.

Timmes, Woosley & Weaver (1995) determined the total elemental abundance for each species. Clearly, some species are depleted from the gas phase to form grains (Graedel, Langer & Frerking 1982) and the initial abundances given to NAHOON need to account for this. A percentage was therefore removed from the initial gas phase abundances following Flower & Pineau des Forêts (2003) (see Table 3). The resulting initial abundances increase smoothly and monotonically with metallicity, which is a reflection of the elemental evolution of the Galaxy. These abundances, before applying depletion, are listed in Table 2, and the electron abundances are set to be the sum of the initial ions abundances. All species are shown with respect to atomic H.

Apart from the atomic and molecular species, the chemical network that we will apply considers grains; so their abundances need to be computed as well. These can be directly determined from the depletion factors that we applied, listed in Table 3. We assume two dust compositions: carbonaceous grains (all depleted carbon) and silicate material (all other depleted elements), and we calculate the total mass of each composition. The resulting dust-to-gas mass ratio is in close agreement with observational studies of the variation of this quantity with metallicity (Reshetnikov 2000; Galametz et al. 2011). The total dust volume can be derived from this by applying densities of 3.5 and 1.8 g cm⁻³ for silicate and carbonaceous material, respectively (Li & Greenberg 1997). Assuming a spherical grain shape and a grain size distribution proportional to $n_{\text{grain}}(r) \propto r^{-3.5}$ (Mathis, Rumpl & Nordsieck 1977), the number density of grains can be calculated. Here we assume two grain sizes: large grains represented by $r = 0.1 \mu\text{m}$ which cover the range from 0.05 to

Table 1. Solar abundances (Asplund et al. 2009)

X	$\log \epsilon(X)_{\odot}$
H	12.00
He	10.93
C	8.43
N	7.83
O	8.69
F	4.56
Na	6.24
Mg	7.60
Si	7.51
P	5.41
S	7.12
Cl	5.50
Fe	7.50

Table 2. Initial elemental abundances with respect to H nuclei for model (4).^a

Species	[Fe/H]					
	-2.5	-2.0	-1.5	-1.0	-0.5	0.0
H	1.00(+00)	1.00(+00)	1.00(+00)	1.00(+00)	1.00(+00)	1.00(+00)
He	0.08(+00)	0.08(+00)	0.08(+00)	0.08(+00)	0.08(+00)	0.08(+00)
N	9.21(-08)	2.05(-07)	4.97(-07)	1.53(-06)	1.50(-05)	5.62(-05)
O	6.12(-06)	1.50(-05)	3.94(-05)	1.11(-04)	3.07(-04)	5.84(-04)
F	2.70(-10)	5.55(-10)	1.46(-09)	6.16(-09)	2.50(-08)	6.81(-08)
C ⁺	1.22(-06)	3.34(-06)	1.09(-05)	4.70(-05)	1.82(-04)	3.39(-04)
Cl ⁺	5.30(-10)	2.49(-09)	7.30(-09)	2.33(-08)	1.02(-07)	4.71(-07)
Mg ⁺	3.47(-07)	7.96(-07)	2.05(-06)	5.99(-06)	1.75(-05)	3.67(-05)
Na ⁺	3.03(-09)	7.16(-09)	2.13(-08)	9.59(-08)	5.85(-07)	1.83(-06)
P ⁺	3.91(-10)	1.46(-09)	4.03(-09)	1.31(-08)	6.76(-08)	3.51(-07)
S ⁺	1.10(-07)	3.32(-07)	8.79(-07)	2.38(-06)	7.18(-06)	1.67(-05)
Si ⁺	3.73(-08)	1.30(-07)	4.88(-07)	1.79(-06)	5.99(-06)	2.60(-05)
Fe ⁺	1.00(-07)	3.16(-07)	1.00(-06)	3.16(-06)	1.00(-05)	3.16(-05)
e	1.82(-06)	4.92(-06)	1.54(-05)	6.04(-05)	2.23(-04)	4.52(-04)
Small grains	1.85(-12)	4.81(-12)	1.39(-11)	4.70(-11)	1.55(-10)	3.41(-10)
Large grains	5.78(-15)	1.50(-14)	4.33(-14)	1.46(-13)	4.85(-13)	1.06(-12)
C ⁺ /O	1.99(-01)	2.22(-01)	2.77(-01)	4.23(-01)	5.93(-01)	5.80(-01)
Dust to gas mass ratio	5.40(-05)	1.39(-04)	3.93(-04)	1.26(-03)	3.99(-03)	8.77(-03)
Grain density ^b	3.03(+00)	3.01(+00)	2.97(+00)	2.79(+00)	2.67(+00)	2.77(+00)

^aThe notation $\alpha(\beta)$ stands for $\alpha \times 10^{\beta}$.

^bGrain density is given in g cm^{-3} .

0.25 μm and small grains, ranging from 0.005 to 0.05 μm , represented by a grain with radius of $r = 0.01 \mu\text{m}$.

2.2 Chemical model

The KIDA chemical network kida.uva.2011² is used to describe the gas phase chemistry. This network contains more than 470 atomic and molecular species connected by more than 6000 gas phase reactions. All reactions occur between only two reactants, since molecular clouds are not

² <http://kida.obs.u-bordeaux1.fr/models>

Table 3. Percentage of elemental abundances remaining in the gas phase

Species	Per cent in gas phase
H	100
He	100
N	100
O	70
F	100
C	40
Cl	50
Mg	0
Na	50
P	50
S	80
Si	0
Fe	0.04

dense enough to allow three-body reactions and are exothermic with no or small reaction barriers. In total 13 elements are included: H, He, C, N, O, Na, Mg, Cl, F, S, Si, P and Fe.

KIDA was used in combination with the publicly available numerical code NAHOON to create and integrate the system of rate equations. This code, written in FORTRAN90 and available through the same webpage as the KIDA chemical network, computes the gas phase chemistry of cold dense molecular clouds and uses the solver DLSODE from the ODEPACK package to solve the system of equations. The chemical evolution was computed at fixed astrophysical parameters (which is normally referred as to zero dimension model, 0D) like, for instance, temperature and total H density. In NAHOON, electrons, neutral grains and grains with one electron charge are considered as species and their abundances are also computed. The network includes neutralization reactions between positively charged species with negatively charged grains and reaction between electron and neutral grains (see table 3 in Wakelam et al. (2012) for a complete list of reactions involving grains). The rates of these processes depend on the collision cross-section and are therefore different for our two grain size populations.

The grain surface reaction leading to H₂ is included in an artificial effective way and this is the only grain process which is accounted for.

2.3 Physical conditions

Dense clouds are thought to evolve from diffuse clouds. We therefore first compute the steady state chemistry of a diffuse cloud and use the obtained abundances as initial condition for the simulations of dense clouds, with appropriate physical parameters. Each diffuse cloud simulation starts with all elements ionized, apart from H, N, O, and F, and all in the atomic form.

Our choice of physical parameters is similar to the parameters used in most of gas phase astro-

Table 4. Physical parameters

Parameter	Diffuse cloud	Dense cloud
T	100 K	10 K
n_{H}	$1 \times 10^3 \text{ cm}^{-3}$	$2 \times 10^4 \text{ cm}^{-3}$
ζ	$1.3 \times 10^{-16} \text{ s}^{-1}$	$1.3 \times 10^{-17} \text{ s}^{-1}$
A_{V}	1 mag	30 mag

chemical models. For easy comparison we chose the parameters as close as possible to the ones used by Wakelam et al. (2012), where the NAHOON program and KIDA network was presented. For dense clouds, the total H density is $2 \times 10^4 \text{ cm}^{-3}$, temperature T is 10 K, visual extinction A_{V} is 30 mag and the cosmic ray (CR) ionization rate ζ is chosen to be $1.3 \times 10^{-17} \text{ s}^{-1}$. For clouds of such high visual extinction CR-induced photons are the dominant radiation source and similar results are expected using other high values for A_{V} . The dependence on ζ will be discussed in more detail in Section 3.8. The physical parameters for both diffuse and dense clouds are summarized in Table 4. Unless explicitly stated, all simulations were run with this set of physical parameters. The abundance of He does not vary with respect to the metallicity. All simulations were performed for 10^8 yr, when steady state is expected to be already reached.

3 RESULTS AND DISCUSSION

3.1 Influence of elemental model

As explained in Section 2.1, different sets of initial conditions could be obtained from the calculations by Timmes, Woosley & Weaver (1995). Figure 2 plots the chemical evolution of a number of selected species for these four models. Additional depletion of the elements according to Table 3 has been applied. The metallicity is $[\text{Fe}/\text{H}] = -2.5$ in all cases. Since the models give similar elemental abundances at solar metallicity and deviation is largest for $[\text{Fe}/\text{H}] = -2.5$, these results should show the strongest effect. The figures show very similar behaviour for all species, except for N_2 and HC_3N . The abundance of nitrogen-bearing species is much higher in the models with convective overshoot for $[\text{N}/\text{Fe}]$ (models 2 and 4), since the amount of available nitrogen is several orders of magnitude higher.

The results presented in the remainder of this section apply model (4) to obtain the initial elemental abundances with additional depletion due to the formation of grains. The percentages of elements remaining in the gas phase are given in Table 3. All simulations were run using the physical parameters summarized in Table 4.

Given a set of elemental abundances, different scenarios can be for the initial conditions in

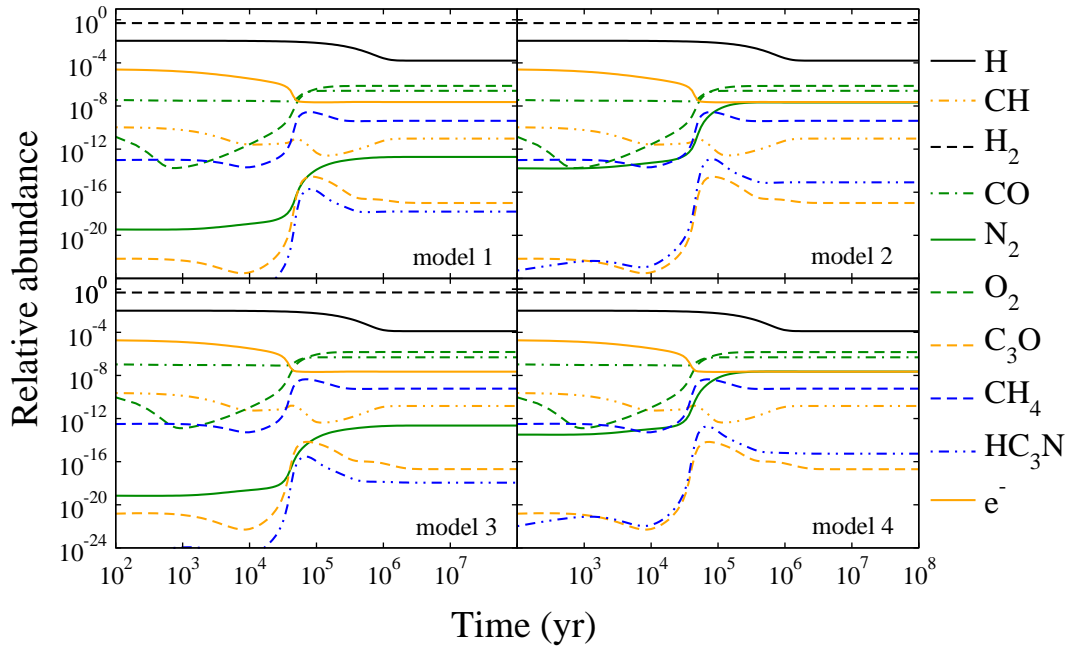


Figure 2. The chemical evolution of a dense molecular cloud for $[\text{Fe}/\text{H}] = -2.5$. The initial elemental abundances are determined from four different models taken from Timmes, Woosley & Weaver (1995).

which these elements exist (ionized, atomic, or molecular form). Here we introduce three possible scenarios and chose one of them to present the results. Figure 3 shows the evolution of important species for two extreme metallicities according to the following scenarios: scenario 0 represents conditions typically used when simulating a dense cloud: all species ionized and hydrogen completely in molecular form; in scenario 1, we first simulate the evolution of diffuse clouds and use the steady state abundances as initial condition for dense clouds; scenario 2 is similar to scenario 1 but here the final abundances of H and H_2 obtained from the dense cloud simulation are taken as initial abundances for another round of dense cloud simulation. The latter scenario is normally chosen when one wants to study the effect of the H abundance on chemical evolution. The steady state is more or less the same for all cases, but it is reached in different ways. For solar metallicity, the absence of H atoms (scenarios 0 and 2) pushes the chemical evolution to later times. For $[\text{Fe}/\text{H}] = -2.5$ scenario 0 is very different from the other scenarios. The results presented in the remainder of the paper are based on scenario 1.

3.2 Metallicity dependence

The chemical evolution of a few species that are crucial in the chemical network is shown in Fig. 4. Clear differences in evolution can be observed as a function of metallicity. An obvious difference is the level of CO that is formed. This is a direct consequence of the amount of C and O available as a function of metallicity. The other oxygen-bearing molecules in Fig. 4 reach steady state much

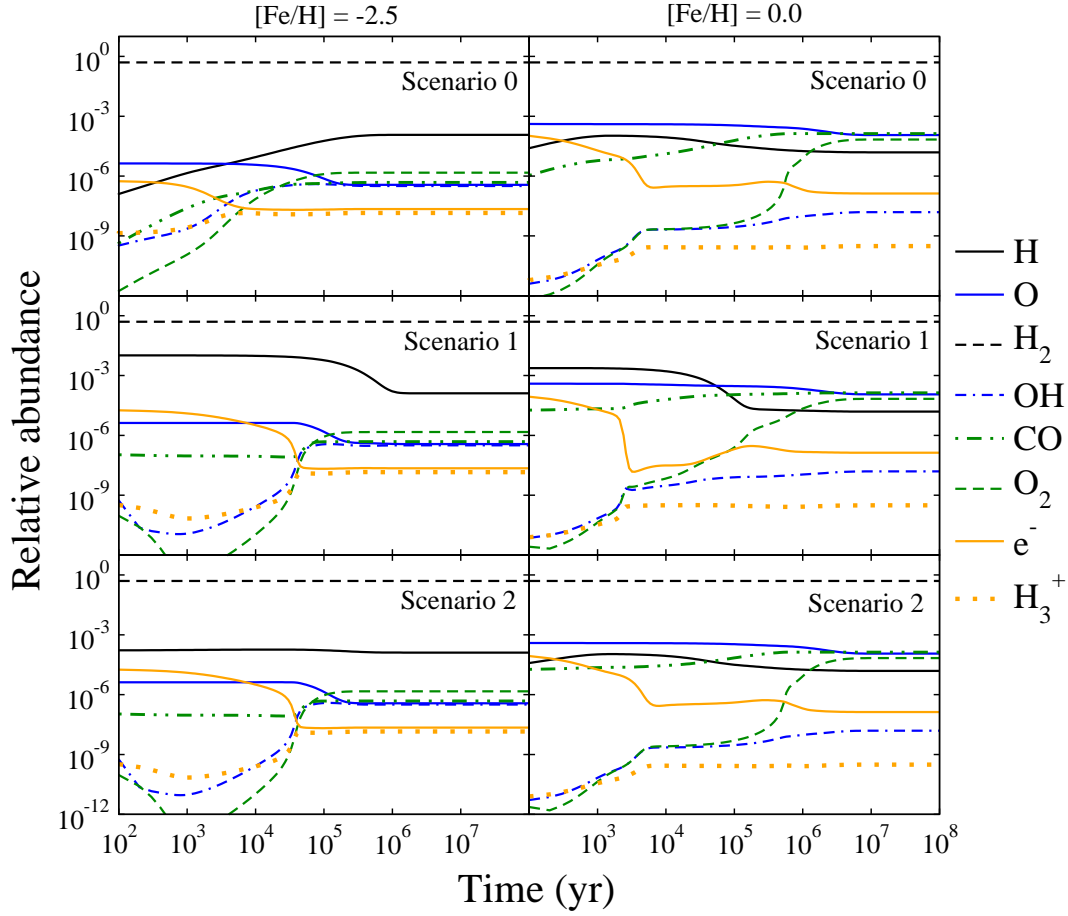


Figure 3. Evolution of important species for the gas phase chemistry according to three different scenarios (see text). Left-hand panels show results for low metallicity whereas right-hand panels show results for high metallicity.

faster for low metallicity as compared to solar metallicity. This is mainly because of the abundance of H_3^+ . This species kick starts the oxygen chemistry by



From H_2O^+ a chain of reactions follows that lead to OH and ultimately to O_2 . Since more H_3^+ is available at low metallicity, as can be seen in Fig. 4 as well, O atoms are much more efficiently converted to O_2 at low metallicities. The main reason that H_3^+ decreases with metallicity is the increase in abundance of CO. CO is the main destructor of H_3^+ at high metallicities, whereas for low metallicities the CO abundance is so low that the reaction $\text{OH} + \text{H}_3^+$ becomes the main destruction pathway for H_3^+ .

Other important species in the gas phase reaction network are electrons. The initial electron density increases with metallicity, since the initial abundance of free electrons is determined by the ionization of metals. So for higher metallicity, more electrons will initially be available. At early times, these electrons are mainly absorbed by H_3^+ and by ionized elements. Since at low metallicity the abundance of H_3^+ is high, this becomes an important reaction. At high metallicities, less H_3^+

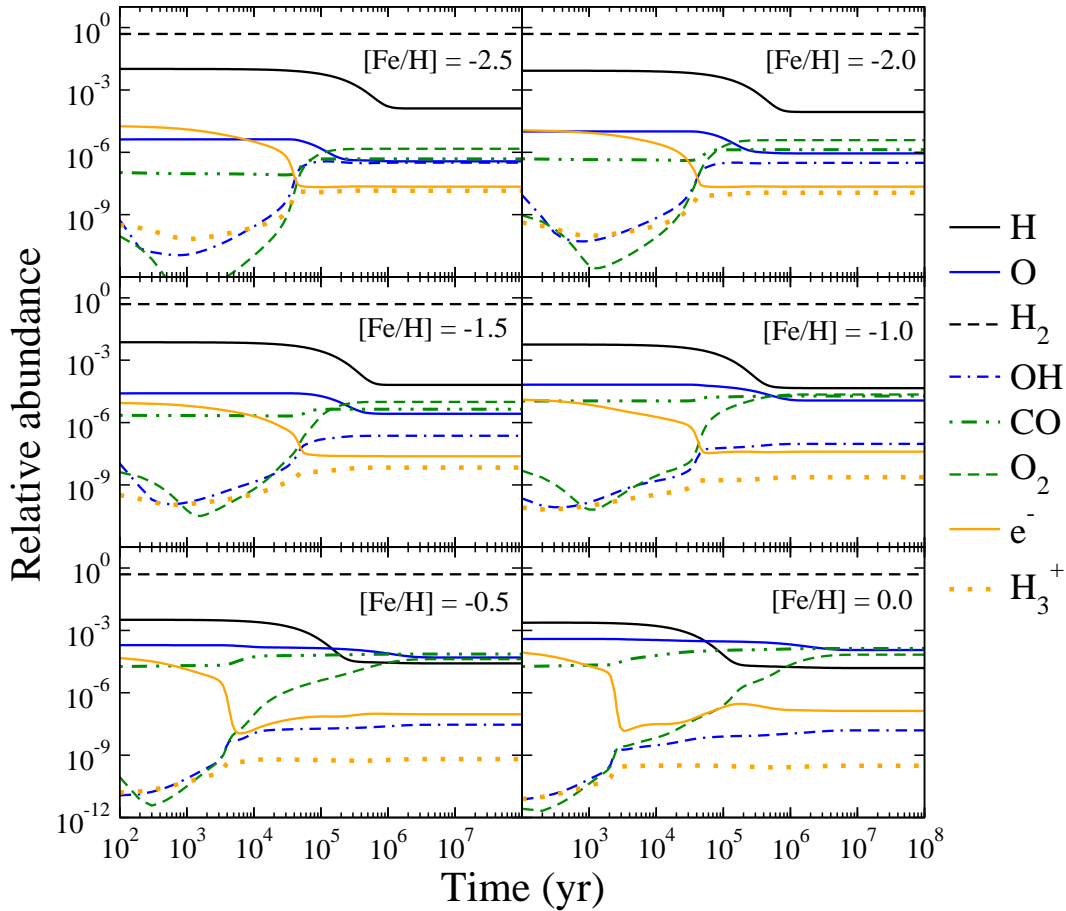


Figure 4. Simulation of the chemical evolution of a molecular cloud for different initial elemental compositions, represented by $[\text{Fe}/\text{H}]$. Results are shown for species that are crucial in the chemical network.

is available, while the initial abundance of ionized elements is higher. Therefore electrons react mainly with charged species. At later times, oxygen reacts efficiently with carbon chain species, destroying them and leading to more free electrons.

Figure 5 shows the gas phase abundance of a few species. One can see that steady state is reached later in the molecular cloud’s life time as the metallicity increases. CO, for instance, has reached its constant final abundance as early as 1×10^5 yr for $[\text{Fe}/\text{H}] = -2.5$ whereas 5×10^5 yrs are required at $[\text{Fe}/\text{H}] = 0$. For N_2 the steady state time-scales are 2×10^5 and 3×10^6 yrs, respectively. It is unclear what the exact lifetime of a cloud is, especially at higher redshift, but it is usually assumed to be $10^5 - 10^6$ yr, after which the cloud becomes dynamically unstable. If this is the case, the cloud has already reached steady state for low metallicity conditions whereas it may not have done so for solar conditions.

Species can be classified as being formed, destroyed, or in steady state on the basis of their relative slopes $[\frac{dn(X)}{dt}/n(X)]$. Visual inspection of the relative slopes shows that steady state is reached when this parameter falls within -1×10^{-8} and $1 \times 10^{-8} \text{ yr}^{-1}$. Figure 6 shows this classi-

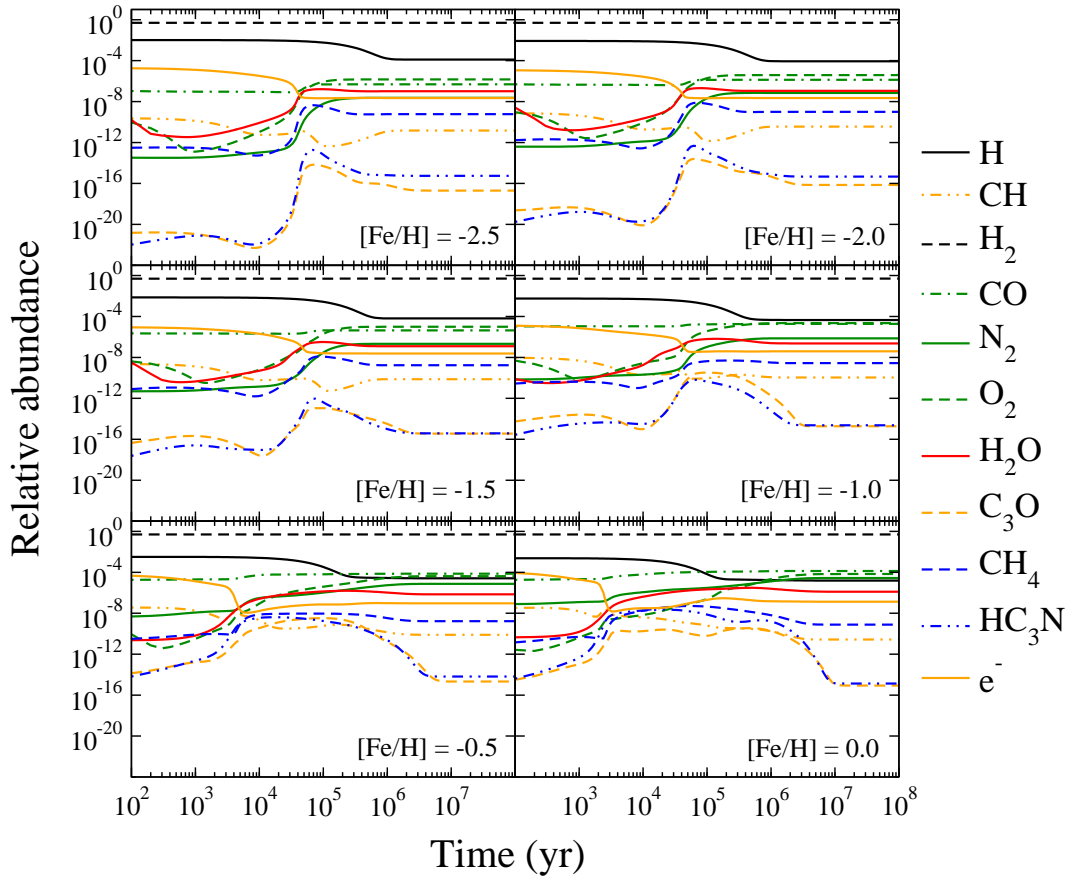


Figure 5. Simulation of the chemical evolution of a molecular cloud for different initial elemental compositions, represented by $[\text{Fe}/\text{H}]$. Results are shown for simple molecules, which are representative of the gas phase chemistry.

fication in terms of percentage for four times and all six metallicities. Generally, three regimes can be distinguished: species are first predominantly formed, some reach a maximum abundance and later become predominantly destroyed and finally in steady state. We see that the second and third regimes are reached earlier for low metallicity than for high metallicity. This can be explained by the abundances of H_3^+ and O. At low metallicity, the high H_3^+ abundance leads to a fast formation of species; an example of this is the oxygen chemistry discussed earlier. At high metallicity, the high O abundance aids in the destruction of species at late times, which makes the destruction process longer. Steady state is already completely reached at 10^8 yr for all metallicities.

3.3 Oxygen chemistry

This section discusses the behaviour of oxygen-containing molecules as a function of redshift. The two most important reservoirs for elemental oxygen in molecular clouds are water and carbon monoxide. Water is predominantly formed through grain surface chemistry, which is not included in our model and the main reservoir of oxygen will therefore be CO in our models. We will return to the formation of H_2O at the end of this section.

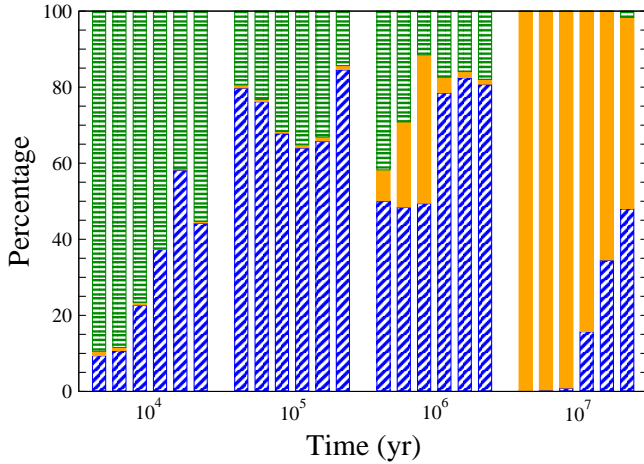


Figure 6. Percentage of molecules being destroyed (blue, oblique line), formed (green, horizontal line), or in steady state (gold, solid) at different moments of the molecular clouds life time for six different metallicities: from left to right ranging from $[\text{Fe}/\text{H}] = -2.5$ to 0.0 . Species are considered in steady state if their relative slope satisfies $-10^{-8} < \frac{dn(X)}{dt}/n(X) < 10^{-8}$.

Figure 7 plots the contribution of the different species to the total oxygen budget. This is done for 24 different situations: for all six metallicities at 10^5 , 10^6 , 10^7 , and 10^8 yr. Our chemical network involves 97 oxygen-bearing species both neutral and ionized ones. Only four species are needed to account for at least 90% of all available oxygen in all 24 situations: CO, O, OH, and O₂. In the previous section we have already discussed part of the oxygen chemistry and how H₃⁺ starts the reactions to convert O to OH and finally O₂. This can also be seen again in Figure 7. Molecular oxygen holds around 40% of all elemental oxygen in molecular clouds with low metallicity. This percentage increases with time. However, this behaviour changes as the metallicity increases. In environments of solar metallicities most of the O is in the atomic form, for early times, while for late times, the oxygen is almost equally shared between the three main O-containing species: O, O₂ and CO. The contribution of CO to the overall oxygen budget increases with metallicity. This is mainly because of the increase in C/O ratio. Figure 8 shows how the C/O ratio increases with metallicity, but always stays below unity. This means the amount of elemental carbon is the determining factor in maximum amount of CO which is formed. The CO contribution to the oxygen budget at late times follows the C/O ratio closely, indicating that indeed nearly all carbon is contained in CO.

On the basis of our models, one might suggest that the gas phase abundance ratio of O₂/CO as a function of metallicity would be a good observational diagnostic to test the validity of our models. Unfortunately, cold O₂ is very hard to observe since it has no permanent dipole, thus it is impossible to use O₂/CO as a test of our model.

Molecular and elemental oxygen are both precursors for the formation of water ice through

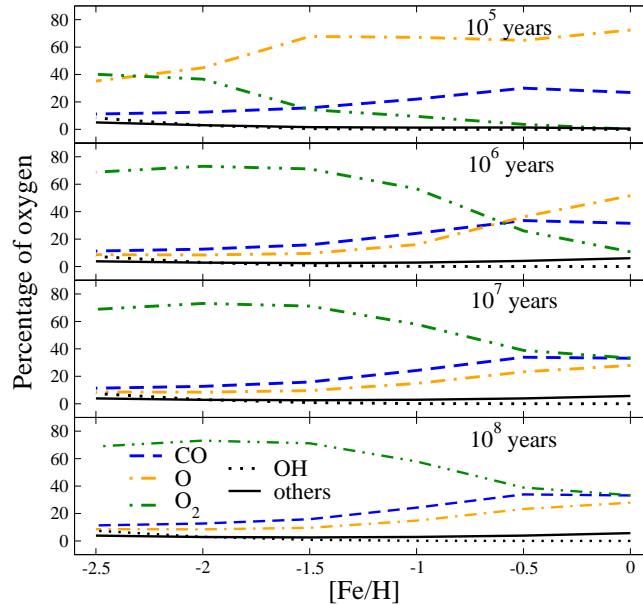


Figure 7. Contribution of different oxygen-bearing species to the total oxygen elemental abundance as a function of $[\text{Fe}/\text{H}]$ for four different times. Only the most abundant species that together account for at least 90% of oxygen are shown.

grain surface reactions. Water can form by different surface mechanisms as was postulated by Tielens & Hagen (1982): through the hydrogenation of O, O_2 , and O_3 . Recent experimentally studies have shown that these three routes can indeed lead to the formation of H_2O (Ioppolo et al. 2008; Miyauchi et al. 2008; Cuppen et al. 2010; Dulieu et al. 2010; Romanzin et al. 2011). Hydrogenation of O_2 and O_3 have H_2O_2 and OH as intermediates whereas O hydrogenation only has OH as intermediate. OH can react further with H or H_2 to form H_2O (Oba et al. 2012). The exact route will determine the amount of formed H_2O_2 , which was recently detected in ρ Oph A (Bergman et al. 2011) as well as the deuterium fractionation and therefore the $\text{HDO}/\text{H}_2\text{O}$ ratio. The freeze-out of O_2 on to grains can also explain the low detection of gas phase O_2 in ρ Oph A (Liseau et al. 2012). Although grain surface chemistry is not included in our models, we can speculate on the formation route based on the gas phase composition, since the reactants for surface reactions reach the grain surface by impinging from the gas phase (Cuppen & Herbst 2007). Since at low metallicity, oxygen is predominantly present in the form of O_2 , the O_2 hydrogenation route is the most likely reaction channel leading to the formation of water ice, especially since the abundance of atomic hydrogen is relatively high because of the low grain density. At solar metallicity, the formation route of $\text{O} + \text{H}$ becomes more likely, since here O atoms dominate. In the intermediate regime, O_3 hydrogenation could be more important, since here O and O_2 can react to form O_3 . Moreover, the atomic hydrogen abundance is also lower, allowing the oxygen species to react before new H atoms land on the surface.

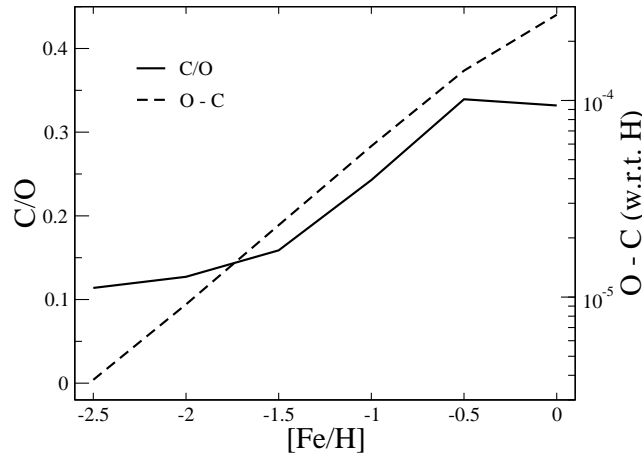


Figure 8. C/O ratio versus [Fe/H] (solid line) and the difference between O and C initial abundances (dashed line). Data are shown after depletion of the elements.

3.4 Nitrogen chemistry

Another element of interest is nitrogen. Nitrogen is an important element in many biomolecules. Its chemistry might give hints whether it will be chemically available for the formation of more complex molecules. N_2 is for instance fairly inert, whereas NO is much more reactive; NH_3 is somewhere in between. Our network contains 123 N-bearing species. Figure 9 shows the contribution of the species to the total nitrogen budget. Again only a handful species is needed to account for a minimum of 90% of the total nitrogen; in this case four: N, N_2 , NO, and NH_3 . In most case, however, only one or two species (N and N_2) are already enough to account for almost the totality of the nitrogen atoms. NO and NH_3 are mostly important at low metallicities, especially for early times. Figure 9 shows the elemental evolution of the Galaxy along the x-axis, while the time evolution can be extracted by comparing the four panels top to bottom. If we analyse the top panel, which represents the moment when it is believed that the molecular clouds start the process of collapse (10^5 yr), it is clear that atomic nitrogen is the main holder of nitrogen, for all metallicities. This is converted to molecular nitrogen in time (second and third panel). This conversion is slower at high metallicity than at low metallicity. Again the difference in oxygen chemistry plays a crucial role, since the main reaction route to N_2 is



followed by



Since the OH abundance is high for low metallicities, this conversion will proceed faster for low metallicity. For high metallicities, nearly all nitrogen is eventually converted to N_2 whereas at

low metallicities a substantial fraction is in the form of NO, N, and NH₃. The nitrogen chemistry completely changes as a function of metallicity.

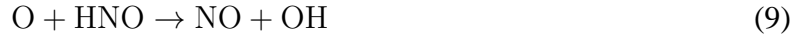
At [Fe/H] = -2.5, the most dominant process which involves NO at late times is its conversion to HNO⁺:



and back



whereas this is completely unimportant at [Fe/H] = 0.0. Here,

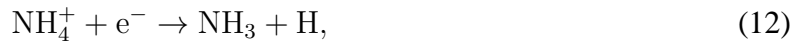


is an important channel to form NO, which is highly improbable at [Fe/H] = -2.5. At solar metallicity, many of the common N-chemical reactions involve phosphorus species or carbon chain molecules whereas these are rather insignificant at [Fe/H] = -2.5.

The nitrogen-bearing species NH₂ can lead to the formation of NH₃ through



and



or be destroyed by O



The first is dominant for low metallicity leading to the formation of NH₃ whereas the latter is dominating at high metallicity.

As explained earlier the gas phase composition can have consequences on possible further surface reactions. Congiu et al. (2012) proved experimentally that hydroxylamine (NH₂OH), a precursor molecule in the formation of amino acids, is efficiently produced by hydrogenation of NO in interstellar ice analogues. This process would be favoured in low metallicity environments because of the higher abundance of NO. On the other hand, atomic nitrogen, available at mainly solar metallicities, could land on the grains and lead to the production of NH₃ through grain surface hydrogen atoms.

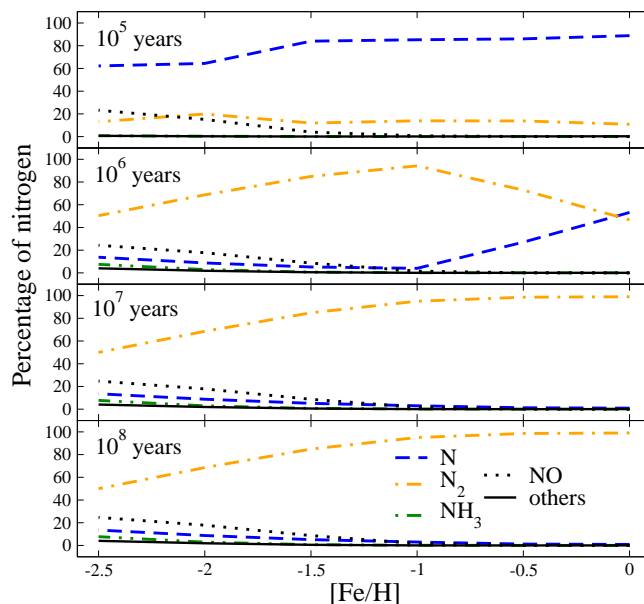


Figure 9. Similar to Fig. 7 but for the nitrogen budget.

3.5 Carbon chemistry

Since the C/O ratio always stays below unity, most of the carbon will be the form of CO. However, still some carbon is available to form more complex species. Figure 10 shows the abundance of species with the general formula C_nH (top panels), C_nH^+ (middle panels) and C_nH^- (bottom panels) at the two extreme metallicities. The figure shows that for $[Fe/H] = -2.5$ the abundance builds up more slowly than for $[Fe/H] = 0.0$. Probably, because less carbon is available which slows down the chemistry. This also results in a lower peak abundance. So for the more complex species the chemistry is slower; contrary for the small species where the chemistry is faster for low metallicity due to the higher concentration of H_3^+ .

For the positively charged species a weak odd-even behaviour can be observed, where the odd species (in number of C) are more abundant. The neutral and negatively charged species do not appear to show this dependence. After approximately 10^6 yr, the abundance quickly drops for solar metallicity and the final abundances are below the $[Fe/H] = -2.5$ values. This is due to the destruction of neutral carbon species by atomic oxygen. For low metallicity, most of the O atoms are locked up in O_2 . Moreover, the elemental oxygen abundance is lower to begin with. For other carbon species similar trends can be observed, but these are not plotted here.

Figure 11 plots the abundance of carbon-bearing species versus number of carbon atoms in the molecule. This can be taken as the length of the carbon chain, although cyclic structures like $c-C_3H$ and C_6H_6 are included as well. This is plotted at four different times for each metallicity.

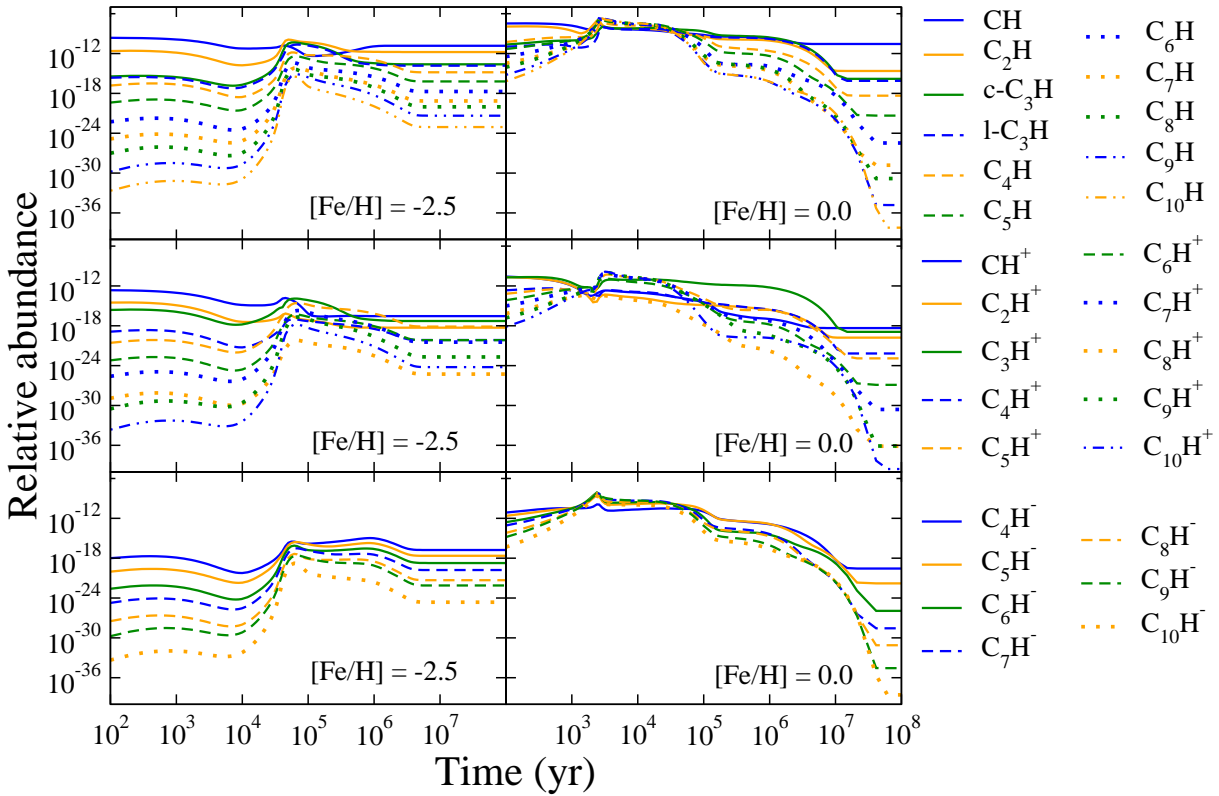


Figure 10. Evolution of carbon-bearing species with general formula C_nH (top panels), C_nH^+ (middle panels) and C_nH^- (bottom panels) as a function of time for $[Fe/H] = -2.5$ (left-hand panels) and $[Fe/H] = 0.0$ (right-hand panels).

There is a decreasing behaviour as can be expected since small molecules are the precursors for the larger ones.

At 10^5 yr, the plots are all more or less the same at first glance. The total amount of carbon bearing species however increases with metallicity, which seems logical since more carbon is available. This increase mostly occurs for the short carbon chains. At later times, a clear drop in the large molecules can be observed, especially for high metallicity. So contrary to what one might initially expect, high metallicity leads to less chemical complexity. This is mainly due to the high oxygen abundance. Graedel, Langer & Frerking (1982) also observed a decrease in carbon chains as a function of the number of metals in the gas phase. This was attributed to destruction by electrons. Free electrons are formed through the ionization of metals. So with more metals, more electrons will be available and a larger fraction of the molecular ions will be destroyed. Graedel, Langer & Frerking (1982) found that better agreement with observations is obtained under “low metal” conditions. For this reason astrochemical simulations are usually performed under these “low metal” conditions, where a large fraction of the gas phase metals are depleted into grains and mantles (Graedel, Langer & Frerking 1982; Flower & Pineau des Forêts 2003). Please notice that in our simulations we performed this depletion as well. So our high metallicity corresponds

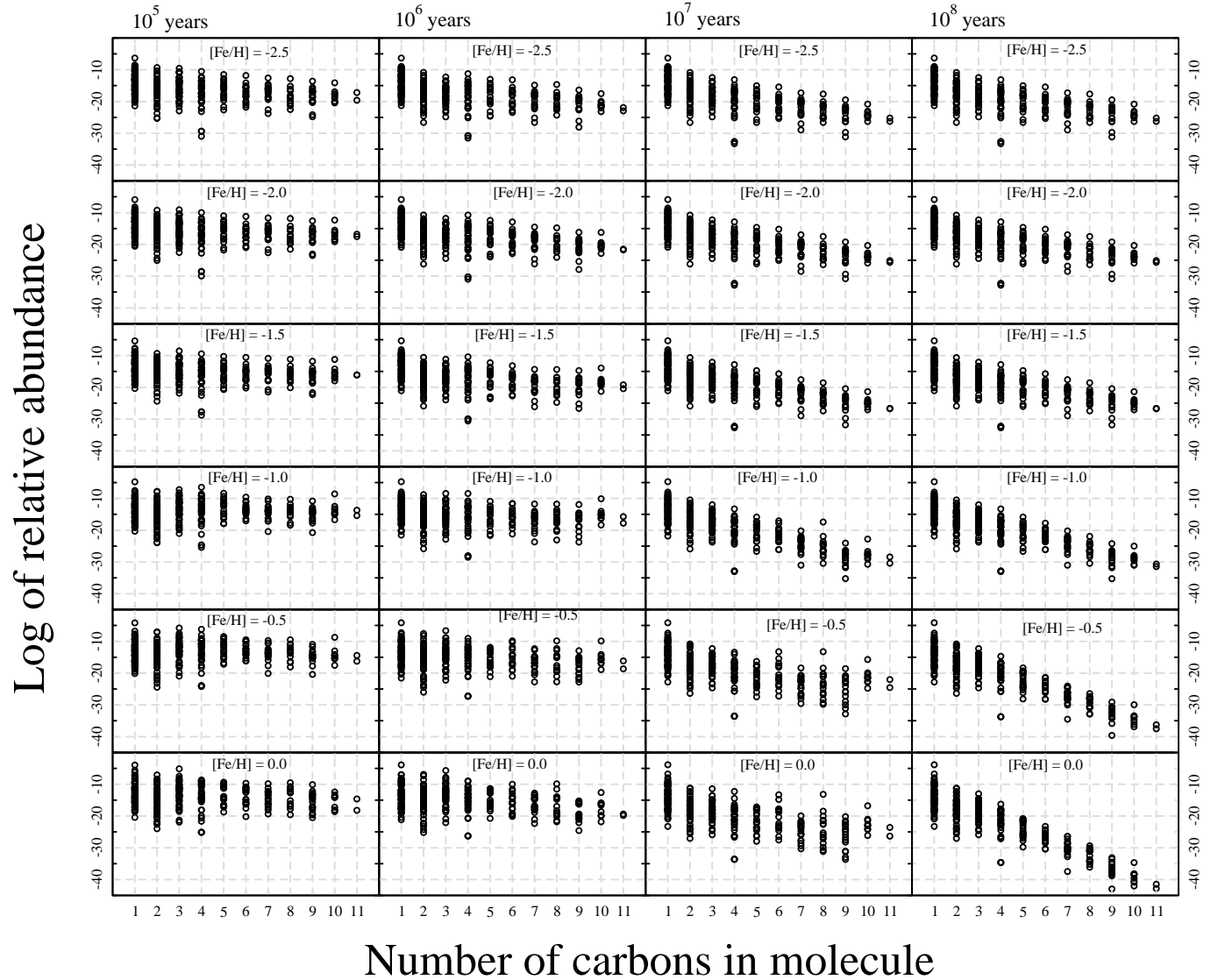


Figure 11. Effect of metallicity on carbon chain length. The abundances of carbon-bearing molecules are shown for four different times (10^5 , 10^6 , 10^7 , and 10^8 yr) according to the number of carbons in the molecules.

more to the “low metallicity” conditions applied in other papers, since there only one metallicity (solar) is normally considered. As mentioned in Sec. 3.2, ionized carbon chain species are mainly destroyed by oxygen at late times and high metallicity condition. This reaction leads to more free electrons, which will react with neutral carbon chain species. The final result is a continuous decrease in carbon chain species and increase in electron abundance.

Similar results have been described by Millar & Herbst (1990) after performing pseudo-time-dependent models to simulate the chemistry of dark clouds located in our Galaxy and in the Large and Small Magellanic Clouds (LMC and SMC, respectively). They found that the abundances of hydrocarbons vary in an unexpected way as one goes from an environment of higher metal abundance (Galaxy) to lower ones (LMC and SMC). It was expected that the abundances of hydrocar-

bons would also decrease in the same order, following the availability of elements. However, they found that the atomic oxygen destroys the hydrocarbons in accordance with our results. Moreover, they found the abundance of atomic O to depend on the quantity O–C instead of O/C, which can be seen in Fig 8. The lower metallicity $[\text{Fe}/\text{H}] = -2.5$ has also the lowest O–C value although the O/C ratio is also the highest one. This shows that there is less atomic oxygen available to react and destroy complex species when the metallicity is lower. Figure 4 indeed shows that the abundance of atomic oxygen is lower for $[\text{Fe}/\text{H}] = -2.5$ during all the molecular cloud's lifetime compared to $[\text{Fe}/\text{H}] = 0.0$

3.6 Sulphur chemistry

This section will discuss the sulphur chemistry. Although this element is present in a small number of species, 46 in total, still plays an important role. S-bearing molecules are often used as molecular clocks to predict the age of the sources where it is observed, because of the relatively fast evolution of their chemistry (Charnley 1997; Wakelam et al. 2004). It is widely accepted that in star forming regions the formation of S-bearing molecules is largely determined during the cold collapse phase. Atomic sulphur freezes out on grains and probably forms H_2S . After formation of the protostar, H_2S evaporates from the surface and starts an active chemistry in the warm gas ($T > 100$ K), where it reacts with H to form sulphur atoms which in turn react with the abundantly present OH and O_2 to form SO and later SO_2 (e.g. Charnley 1997). Since this process occurs on time scales of roughly 10^4 yr the relative amounts of H_2S , SO and SO_2 can be used as a chemical clock for warm gas in hot cores and hot corinos, but also in outflows and shocks (Pineau des Forets et al. 1993; Chernin, Masson & Fuller 1994; Bachiller & Perez Gutierrez 1997).

Since we limit our study to the cold cloud stage, it would be interesting to see how much S is available for depletion on to grains where it can form H_2S , which will kick start the sulphur chemistry at a later stage. Figure 12 shows the main sulphur-bearing species as a function of metallicity. Here three species are needed to account for a minimum of 90 % of the total sulphur abundance. At early times, all sulphur is in the elemental form, while in late times, most of the sulphur ends locked up in SO_2 , having SO as intermediary species. The amount of conversion increases with metallicity: for low metallicity S remains the dominant form, for solar metallicity SO_2 contains most of the sulphur, whereas at intermediate metallicity SO is more important. This is surprising since SO usually forms from reaction of S with OH and O_2 and Figure 7 shows that both species are predominantly present at low metallicity. The key reactions to explain this

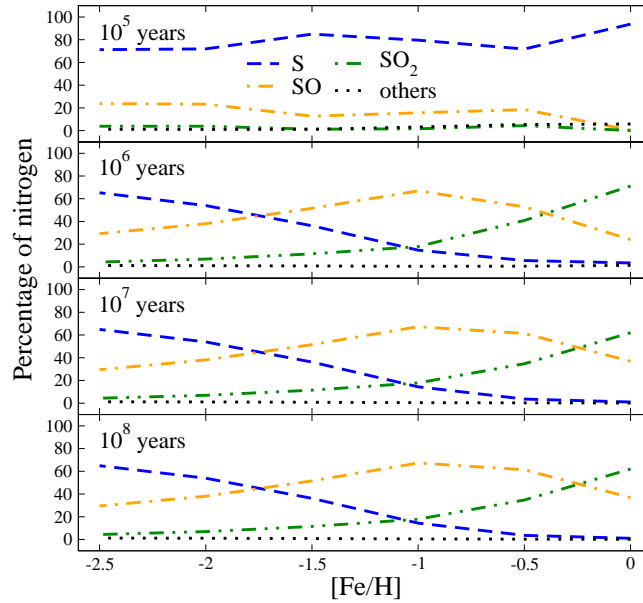


Figure 12. Similar to Fig. 7 but for the sulphur budget.

behaviour are however the follow up reactions with SO as one of the reactants:



and



The first moves the systems down in the $\text{S} \rightarrow \text{SO} \rightarrow \text{SO}_2$ chain, whereas the latter continues the chain reaction. From Figure 4 it can be easily understood that the first reaction dominates at low metallicity, whereas the latter is the main reaction route at solar metallicity, converting a large part of the sulphur into SO_2 . According to Ruffle et al. (1999) the S depletion time scale on grains is 2.5×10^6 yr. Figure 12 shows that within this time frame, a significant fraction of the gas phase S has been converted to SO and SO_2 at high metallicity, which can freeze out on the grains as well. This makes the sulphur chemistry a less reliable clock for these conditions. At low metallicity, on the other hand, much more S is available to form H_2S on the grain surfaces with the S-depletion time frame, with hardly any SO_2 contamination, making it a more clean mechanism at these conditions.

All graphs show that the majority of the species are in neutral form. This is because under these conditions the cloud is shielded from most ionization processes.

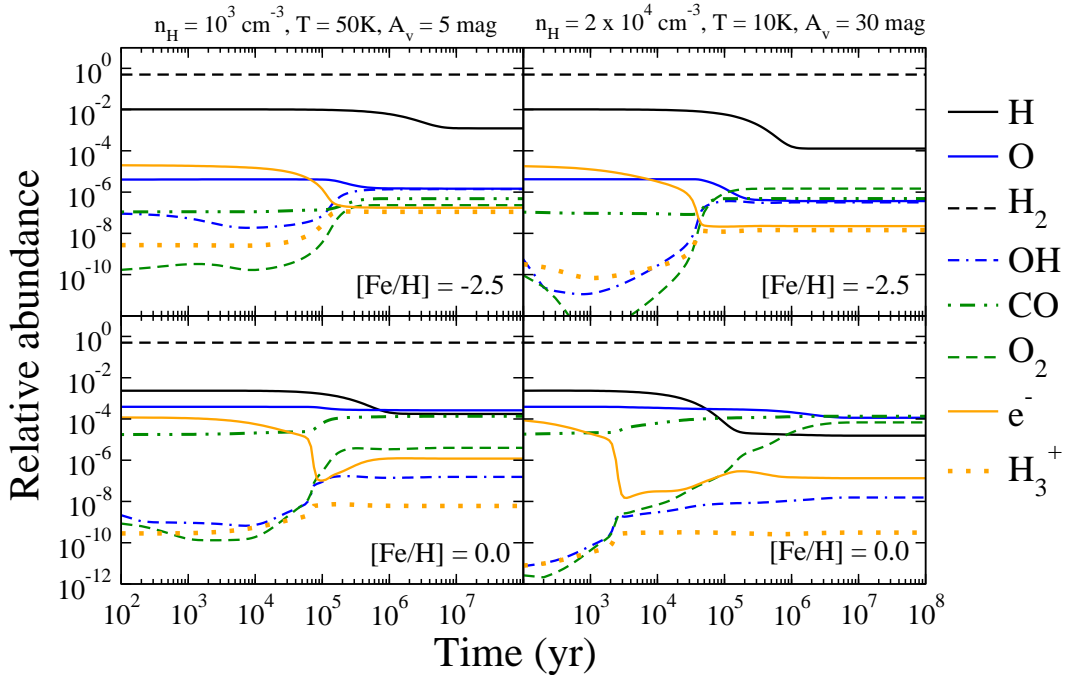


Figure 13. Comparison between lower and higher densities. Left-hand panels: time evolution of diffuse/translucent clouds with total hydrogen density $n_{\text{H}} = 10^3 \text{ cm}^{-3}$, temperature $T = 50 \text{ K}$ and visual extinction $A_{\text{V}} = 5 \text{ mag}$. Right-hand panels: time evolution of dense clouds with the physical parameters described in Table 4. Top panels show results for low metallicities whereas high metallicity is shown on bottom panels. A CR ionization rate of $\zeta = 1.3 \times 10^{-17} \text{ s}^{-1}$ was used in all simulations.

3.7 Density dependence

Extragalactic sources are usually not spatially resolved and the observations consist of contributions by different density regions, mainly those regions of low densities. We therefore performed simulations of a translucent cloud, with a lower total hydrogen density of $n_{\text{H}} = 10^3 \text{ cm}^{-3}$, temperature $T = 50 \text{ K}$ and visual extinction $A_{\text{V}} = 5 \text{ mag}$, to compare to the dense cloud results. This comparison is shown in Fig. 13. The left-hand panels show the time evolution of the translucent cloud whereas the right-hand panels show the evolution of the dense cloud. In both cases the initial chemical composition of the cloud was taken from a diffuse cloud simulation. For the translucent cloud, the chemical time scale remains more or less the same for low metallicities whereas the chemical time-scale is much more constraint for high metallicity. Chemistry starts later because of the lower density, but steady state is reached much faster. The absolute relative abundances are also quite different going from the dense to the translucent cloud. The stable species O_2 decreases whereas all other species increase.

The search for observational evidence of molecules in external galaxies started already a few decades ago. Up to the present date, around 60 molecules have been detected in extragalactic sources (see “<http://www.astro.uni-koeln.de/cdms/molecules>” for an updated list). Most of these molecules are detected in nearby galaxies (e.g. Rickard et al. 1975; Martín et al. 2003). To re-

late our model results to observations, we will first need to relate metallicity to redshift, which depends on the cosmological model applied. Figure 9 in Chiappini et al. (1999) shows this relationship for different cosmologies. For more standard values, a metallicity of $[0/\text{Fe}] = 0.6$, which corresponds to $[\text{Fe}/\text{H}] = -2.5$ according to Timmes, Woosley & Weaver (1995), results in a redshift between 3.8 and 3. Species have been detected at such high redshift and even higher (e.g., Walter et al. 2003; Wagg et al. 2005; Guélin et al. 2007), but fractional abundances have not been derived. The *Herschel* Dwarf Galaxy Survey has observed lines like [CII], [OI], [OIII] and [NII] for low-metallicity galaxies (Madden et al. 2013). Unfortunately, again no abundances have been presented so far. This makes it difficult at the present stage to make a direct comparison between our model results and observations.

3.8 Cosmic ray ionization dependence

CRs play a crucial role on the chemistry of the ISM since they are the main ionization mechanism capable to ionize many of the most abundant species and, therefore, initiating the reaction network. For example, reaction between CRs and H_2 produces electrons



and triggers the formation of H_3^+ in the follow-up reaction:



As discussed in Section 3.2, these are two of the most determining species for the chemical evolution of our molecular clouds. The outcome of our simulations will therefore strongly depend on the value chosen for the CR ionization rate. Unfortunately, this rate is highly uncertain. Theoretical and observational studies give a range that covers orders of magnitude: from 10^{-18} to 10^{-15} s^{-1} ; although recent studies point to a value on the order of 10^{-16} s^{-1} for diffuse clouds and about 0-2 orders of magnitude lower in dense clouds (Indriolo & McCall 2012). Our initial choice of $\zeta = 1.3 \times 10^{-16} \text{ s}^{-1}$ for diffuse clouds and $\zeta = 1.3 \times 10^{-17} \text{ s}^{-1}$ for dense clouds is in accordance with this data.

Figure 14 shows the impact of different values of CRs ionization rate on the evolution of the crucial species. Four different CR ionization rate values, ranging from $\zeta = 10^{-19}$ to 10^{-16} s^{-1} , were chosen to investigate the impact on the chemical evolution at the two extreme metallicities. Each simulation was performed using the parameters described in Table 4 but with the CR ionization rate as noted in the Figure 14. The CR ionization rate in the preceding diffuse cloud simulations was chosen to be one order of magnitude higher.

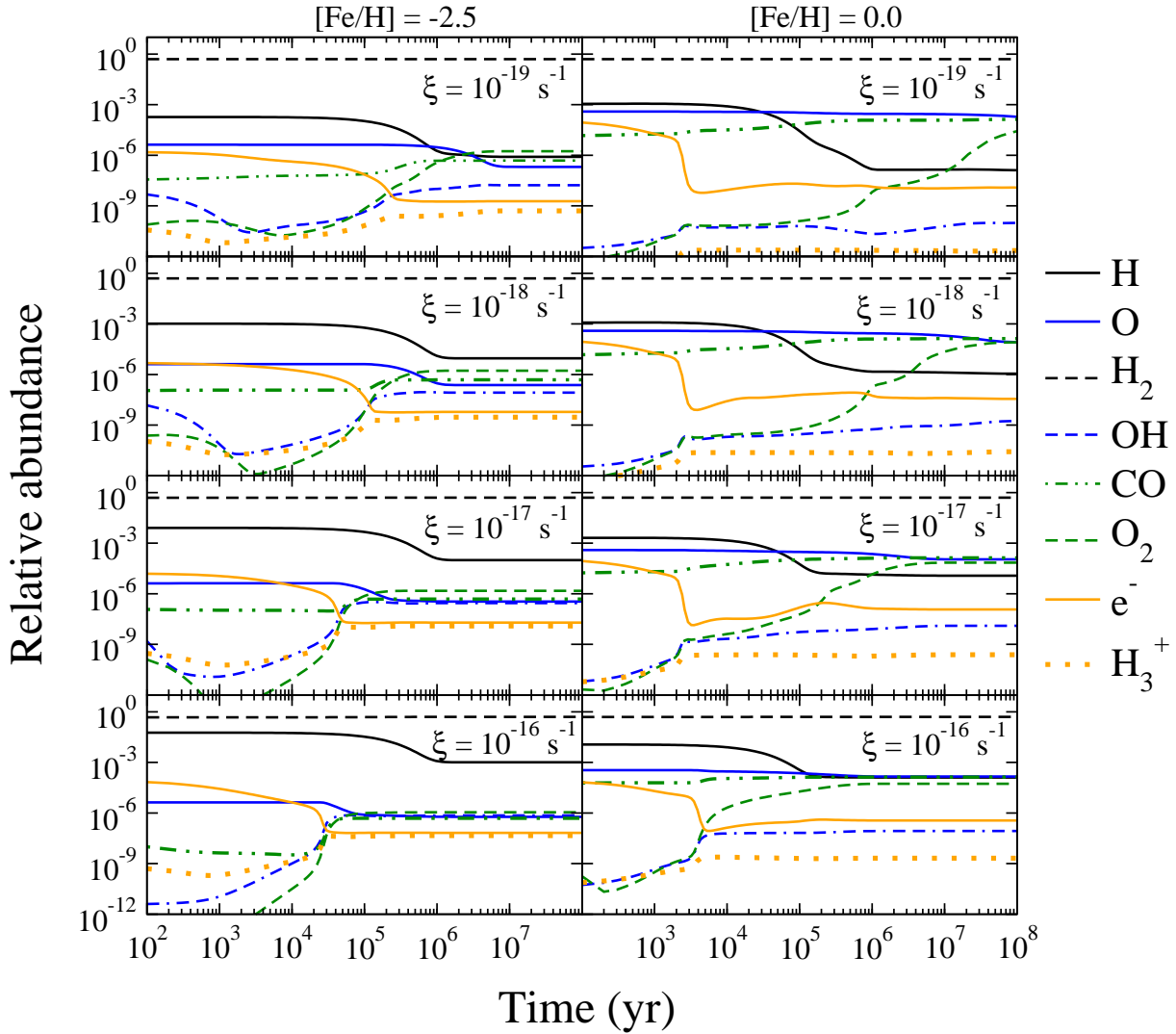


Figure 14. Dependence on the CR ionization rate in the evolution of crucial molecules in dense molecular clouds. Simulations were performed for the two extreme metallicities. The CR ionization rate used is noted and each simulation was preceded by the simulation of a diffuse cloud with CR ionization rate of one order of magnitude higher.

It is clear that the steady state of the considered molecules is reached earlier as the CR ionization rate increases, for both metallicities. The production of e^- and H_3^+ increases with the CR ionization rate as is expected, since these species are direct products of interaction between CRs and H_2 . Their steady state abundance together with OH follows a power-law dependence on the CR ionization rate as can be seen in Figure 15. The abundances of O, O_2 and, CO appear to remain unaffected by the CR ionization rate except for high CR rates in translucent clouds at low metallicity. Notice that for the lowest CR ionization rates at solar metallicity steady state was reached beyond 10^7 yr.

It is well established that the chemistry of dense molecular clouds may present bistability when varying physical parameters like the CR ionization rate and depletion level (e.g., Le Bourlot et al. 1993, 1995; Lee et al. 1998). This phenomenon is suggested to be a mathematical consequence

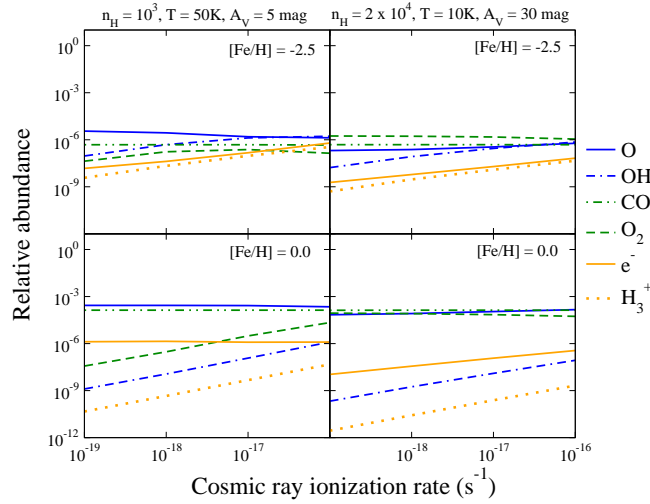


Figure 15. Dependence of the steady state abundance on the CR ionization rate for two different total hydrogen density.

of the non-linearity of the rate equations that describe the chemical evolution of molecular clouds (Shalabiea & Greenberg 1995). Species involved in this phenomenon are H_3^+ , O_2 and S^+ and the reactions connecting them, as described by Boger & Sternberg (2006). In this section we vary both the initial elemental abundance and the CR ionization rate. We see no signs of bistability in Figures 14 and 15, since here the steady state abundances change smoothly with CR ionization rate; the O_2 steady state abundance appears even to be unaffected by the CR ionization rate in most cases, except for the case of low total hydrogen density and high metallicity, where it increases monotonically. Although no sign of bistability was found with the described simulations, this phenomenon could still be present here. To explore the presence of bistable solutions in detail, one needs to perform simulations with a range of random initial conditions. However, such performance is beyond the scope of the present work.

4 CONCLUSIONS

We have studied the role of the elemental evolution of the Galaxy on the chemical evolution of cold and dense molecular clouds. Violent processes leading to the death of stars deliver to the ISM new elements produced in the interior of the stars. Such elements enrich the surrounding gas, which will evolve and form new stars and planetary systems. Therefore, new generations of stars are born with different metallicities. In this paper, we simulate the chemical evolution of molecular clouds from a set of different initial elemental abundances, reflecting the change on the metallicity leaded by the elemental evolution of the Galaxy. Our main results are listed below:

- (1) The changes in gas phase chemistry can be explained by the changes in abundance of three species: electrons, H_3^+ , and O.
- (2) Electrons mainly charge carbon chain species at high metallicity, which in turn will be destroyed by atomic oxygen.
- (3) Since CO is less abundant at low $[\text{Fe}/\text{H}]$ because of the low availability of elemental C and O, H_3^+ can sustain higher abundances. This triggers the formation of OH and O_2 from atomic oxygen. It further destroys SO and PO and facilitates the conversion of NH_2 into NH_3 .
- (4) Because of the low O abundance in general and its quick conversion into O_2 , less O atoms are available at low $[\text{Fe}/\text{H}]$ to destroy large carbon species, to convert SO into SO_2 , and to prevent the formation of NH_3 from NH_2 .
- (5) Higher CR ionization leads to higher abundances of H_3^+ , OH and electrons. The steady state is reached earlier with higher cosmic ray ionization rate.

The new generations of ground-based interferometers, such as ALMA, will increase the sensitivity of observations allowing unequivocal detection of molecules in extragalactic sources, at higher redshifts, forcing a new development of astrochemical models able to take into account the new chemical complexity that will come up with these new facilities. In the near future, it will be possible to have a better comprehension of the chemistry happening in different redshift from the observational point of view, putting the current work to the test.

ACKNOWLEDGMENTS

EMP and HMC acknowledge the European Research Council (ERC-2010-StG, Grant Agreement no. 259510-KISMOL) for financial support. HMC is grateful for support from the VIDI research program 700.10.427, which is financed by The Netherlands Organization for Scientific Research (NWO). EMP also thanks FAPERJ for financial support during the early developments of this research. The authors would like to thank Eric Herbst, Tom Millar and the anonymous referee for interesting discussions and suggestions.

REFERENCES

- Asplund M., Grevesse N., Sauval A. J., Scott P., 2009, *ARA&A*, 47, 481
- Bachiller R., Perez Gutierrez M., 1997, *ApJ*, 487, L93
- Bergman P., Parise B., Liseau R., Larsson B., Olofsson H., Menten K. M., Güsten R., 2011, *A&A*, 531, L8

- Boger G. I., Sternberg A., 2006, *ApJ*, 645, 314
- Cazaux S., Spaans M., 2009, *A&A*, 496, 365
- Charnley S. B., 1997, *ApJ*, 481, 396
- Chernin L. M., Masson C. R., Fuller G. A., 1994, *ApJ*, 436, 741
- Chiappini C., Matteucci F., Beers T. C., Nomoto K., 1999, *ApJ*, 515, 226
- Congiu E. et al., 2012, *ApJ*, 750, L12
- Cuppen H. M., Herbst E., 2007, *ApJ*, 668, 294
- Cuppen H. M., Ioppolo S., Romanzin C., Linnartz H., 2010, *Phys. Chem. Chem. Phys.*, 12, 12077
- Dulieu F., Amiaud L., Congiu E., Fillion J.-H., Matar E., Momeni A., Pirronello V., Lemaire J. L., 2010, *A&A*, 512, A30
- Flower D. R., Pineau des Forêts G., 2003, *MNRAS*, 343, 390
- Galametz M., Madden S. C., Galliano F., Hony S., Bendo G. J., Sauvage M., 2011, *A&A*, 532, A56
- Graedel T. E., Langer W. D., Frerking M. A., 1982, *ApJS*, 48, 321
- Guélin M. et al., 2007, *A&A*, 462, L45
- Herbst E., Klemperer W., 1973, *ApJ*, 185, 505
- Herbst E., van Dishoeck E. F., 2009, *ARA&A*, 47, 427
- Indriolo N., McCall B. J., 2012, *ApJ*, 745, 91
- Ioppolo S., Cuppen H. M., Romanzin C., van Dishoeck E. F., Linnartz H., 2008, *ApJ*, 686, 1474
- Le Bourlot J., Pineau des Forêts G., Roueff E., Flower D. R., 1995, *A&A*, 302, 870
- Le Bourlot J., Pineau des Forêts G., Roueff E., Schilke P., 1993, *ApJ*, 416, L87
- Lee H.-H., Roueff E., Pineau des Forêts G., Shalabiea O. M., Terzieva R., Herbst E., 1998, *A&A*, 334, 1047
- Li A., Greenberg J. M., 1997, *A&A*, 323, 566
- Liseau R. et al., 2012, *A&A*, 541, A73
- Madden S. C. et al., 2013, *PASP*, 125, 600
- Martín S., Mauersberger R., Martín-Pintado J., García-Burillo S., Henkel C., 2003, *A&A*, 411, L465
- Mathis J. S., Rumpl W., Nordsieck K. H., 1977, *ApJ*, 217, 425
- Millar T. J., Herbst E., 1990, *MNRAS*, 242, 92
- Miyauchi N., Hidaka H., Chigai T., Nagaoka A., Watanabe N., Kouchi A., 2008, *Chem. Phys. Lett.*, 456, 27
- Oba Y., Watanabe N., Hama T., Kuwahata K., Hidaka H., Kouchi A., 2012, *ApJ*, 749, 67

- Pereira-Santaella M. et al., 2013, ApJ, 768, 55
- Pineau des Forets G., Roueff E., Schilke P., Flower D. R., 1993, MNRAS, 262, 915
- Reshetnikov V. P., 2000, Astrophysics, 43, 145
- Rickard L. J., Palmer P., Morris M., Zuckerman B., Turner B. E., 1975, ApJ, 199, L75
- Romanzin C., Ioppolo S., Cuppen H. M., van Dishoeck E. F., Linnartz H., 2011, J. Chem. Phys., 134, 084504
- Ruffle D. P., Hartquist T. W., Caselli P., Williams D. A., 1999, MNRAS, 306, 691
- Shalabiea O. M., Greenberg J. M., 1995, A&A, 296, 779
- Tielens A. G. G. M., Hagen W., 1982, A&A, 114, 245
- Timmes F. X., Woosley S. E., Weaver T. A., 1995, ApJS , 98, 617
- Vasyunin A. I., Herbst E., 2013, ApJ, 762, 86
- Wagg J., Wilner D. J., Neri R., Downes D., Wiklind T., 2005, ApJ, 634, L13
- Wakelam V., Caselli P., Ceccarelli C., Herbst E., Castets A., 2004, A&A, 422, 159
- Wakelam V., Herbst E., Le Bourlot J., Hersant F., Selsis F., Guilloteau S., 2010, A&A, 517, A21
- Wakelam V. et al., 2012, ApJS , 199, 21
- Walter F. et al., 2003, Nature, 424, 406
- Wheeler J. C., Sneden C., Truran, Jr. J. W., 1989, ARA&A, 27, 279